ACS APPLIED MATERIALS & INTERFACES

Letter

Rapid and Highly Sensitive Detection of Dopamine using Conjugated Oxaborole based Polymer and Glycopolymer Systems

Keren Jiang, Yinan Wang, Garima Thakur, Yohei Kotsuchibashi, Selvaraj Naicker, Ravin Narain, and Thomas Thundat

ACS Appl. Mater. Interfaces, **Just Accepted Manuscript** • Publication Date (Web): 24 Apr 2017

Just Accepted

ACS Publications

ACS Applied Materials & Interfaces is published by the American Chemical Society.
1155 Sixteenth Street N.W., Washington, DC 20036

Rapid and Highly Sensitive Detection of Dopamine using Conjugated Oxaborole based Polymer and Glycopolymer Systems

Keren Jiang, Yinan Wang, Garima Thakur, Yohei Kotsuchibashi, Selvaraj Naicker, Ravin Narain, and Thomas Thundat**

Department of Chemical and Materials Engineering, University of Alberta, Edmonton, Alberta, T6G 2V4, Canada

ABSTRACT A conjugated polymer interface consisting of an oxaborole containing polymer and a glycopolymer was used for achieving very high selectivity in dopamine (DA) detection. The optimum binding affinity between the polymers promotes the selectivity to DA through a displacement mechanism while remaining unaffected by other structurally related analogs and saccharide derivatives. Real-time detection of DA with very high selectivity and sensitivity has been demonstrated by immobilizing the polymer conjugates on surface plasmon resonance (SPR) and microcantilever (MCL) sensor platforms. Using the conjugated polymer sensing layer, the SPR biosensor was capable of detecting DA in the concentration range of 1×10^{-9} to 1×10^{-4} mol L^{-1} while the MCL sensor showed a limit of detection (LOD) of 5×10^{-11} mol L^{-1}. We find that the sensing mechanism is based on DA-induced reversible swelling of the conjugated polymer layer and this allows regeneration and reuse of the sensor multiple times. Also, we conclude that SPR is a suitable sensor platform for DA in-line detection at clinical level considering the detection time and stability, while MCL can achieve a much lower LOD.

KEYWORDS: Dopamine detection, Selectivity, Oxaborole polymer, Glycopolymer, Microcantilever, Surface plasmon resonance

Dopamine (DA) is a simple organic chemical in the catecholamine family which plays a critical role in the function of the central nervous system (CNS), endocrine system and cardiovascular system. Monitoring the concentration level of DA has attracted a great deal of attention since its level can indicate various types of diseases, such as Parkinson's disease, schizophrenia and dementia[1–3]. Much effort has been focused on the development of techniques for highly selective and quantitative detection of DA. In the past decades, several analytical methods, such as high performance liquid chromatography (HPLC)[4], capillary electrophoresis[5], fluorescence[6] and electrochemical methods[7,8], have been developed for DA level monitoring, but they require long sample-preparation time and well-trained operators. Novel sensors utilizing field-effect transistor (FET)[9], nanoparticles[10] and conducting polymers[9,11] have been developed for DA detection, but they require complicated sensor surface functionalization and lack long-term stability. DA level in biological samples is in the range of 10^{-9} to 10^{-5} mol L^{-1}(M), with an excess of epinephrine (EPI), ascorbic acid (AA), uric acid (UA) and other compounds[11,12]. Thus, development of a real-time detection system for DA that is highly specific and sensitive is still needed. Although there are many sensitive sensor platforms, they require selective receptor layers for obtaining selectivity in detection.

Boronic acid is well known for its interaction with molecules having a cis-diol configuration to form stable cyclic esters[13]. A well-defined block copolymer poly(*N*-isopropylacrylamide-*st*-5-methacrylamido-1,2-benzoxaborole) (P(NIPAAm-*st*-MAAmBO)) has been synthesized by reversible addition-fragmentation chain transfer (RAFT) polymerization by Narain and coworkers[14]. Dopamine, due to the nature of the catechol group, was reported to have a binding constant (~18000 K mol^{-1}) over two orders of magnitude higher than that of the cis-diol containing compounds (~100 K mol^{-1}), such as glucose, fructose, and mannose etc., toward the boronic groups[15]. However, due to the relatively low physiological level of DA as compared to other chemicals such as saccharides[2,16], a highly-selective

sensing layer is needed for DA detection. It has been demonstrated that glycopolymers can form stable structure with boroxol containing compounds[14,17]. Due to their structural difference, the binding affinity between P(NIPAAm-*st*-MAAmBO) and glycopolymer (poly(2-lactobionamidoethyl methacrylamide) (PLAEMA), which has two cis-diol unit in each side-chain, is estimated to be lower than that of DA, but higher than that of monosaccharides[15]. This makes the conjugated P(NIPAAm-*st*-MAAmBO) and PLAEMA layer much less reactive to non-specific saccharides or other structural analogs, leaving only DA binding to P(NIPAAm-st-MAAmBO) by the displacing PLAEMA.

In this work, we describe a highly selective interface for DA detection and we demonstrate it in two different sensor platforms, namely surface plasmon resonance (SPR) and microcantilevers (MCL). SPR is a sensitive technique for fast and label-free detection of chemical and biological analytes[18,19]. Microcantilever sensor based on mechanical bending, on the other hand, utilizes changes in surface stress due to surface adsorption[20]. However, both the SPR and the MCL sensors require functional coatings for obtaining selectivity in sensing. With functionalized sensing layers, both sensor platforms have been utilized for sensing and diagnosing applications in solution environments that include whole cell recognition, protein interaction, glucose sensing, heavy metal detection, etc.[21–23]. The conjugated polymer layer consisted of P($NIPAAm_{149}$-*st*-$MAAmBO_{19}$) (MAAmBO content: 12 mol%, M_n: 13200 g mol^{-1}, M_w/M_n=1.27) and P($LAEMA_{21}$) (M_n: 10000 g mol^{-1}, M_w/M_n=1.1)[14]. In addition to the DA detection in buffer solutions, this conjugated polymer layer is evaluated for specificity in the presence of cross-reacting analytes such as saccharides, EPI, AA and UA. We have investigated the selectivity, sensitivity, and the polymer layer swelling of this conjugated polymer system. The possible regeneration of the polymer interface has also been evaluated.

The gold-coated SPR and MCL sensor chips were carefully cleaned using piranha solution (H_2SO_4 and H_2O_2, 3:1 in volume) and rinsed by aliquots of water and ethanol and dried by nitrogen before any surface functionalization process. The polymer functionalization was performed in a three-step method. First, P(NIPAAm$_{149}$-*st*-MAAmBO$_{19}$) was immobilized to the gold-coated surface of the sensor for forming a self-assembled monolayer (SAM) via thiol-Au covalent bond through the dithioester group at the polymer terminal. The second layer of P(LAEMA$_{21}$) was conjugated to the sensor substrate by the oxaborole-diol interaction as described previously. After rinsing with PBS, the chip was treated with thiolated poly(ethylene glycol) (PEG) to block any uncovered gold surface in order to avoid non-specific adsorption. A PEG functionalized chip was used as a reference to eliminating noise and other systematic errors (by common mode rejection). SPR reflection angle was measured by Navi 200 instrument (BioNavis, Finland) and the mechanical bending of microcantilevers was measured by means of a multiplexed optical beam deflection setup. SPR sensorgram and MCL deflection signals monitored as a function of time during the injection of DA samples. ^{11}B NMR was performed to confirm the DA displacement reaction with P(NIPAAm$_{149}$-*st*-MAAmBO$_{19}$) and P(LAEMA$_{21}$) conjugates. The topography of the conjugated polymer functionalized chip before and after DA injections was acquired using an atomic force microscopy (AFM) for investigating surface morphology evolution due to adsorption.

Figure 1 shows the DA detection mechanism using the covalent interaction between DA and P(NIPAAm$_{149}$-*st*-MAAmBO$_{19}$) on both SPR and MCL sensor platforms. The structures and schematics of the polymers and DA are listed in Figure 1A. The reaction process is briefly described in Figure 1B where the DA binding to P(NIPAAm$_{149}$-*st*-MAAmBO$_{19}$) resulting in the displacement of the previously conjugated P(LAEMA$_{21}$). The DA displacement swells the P(NIPAAm$_{149}$-*st*-MAAmBO$_{19}$) on the SPR sensor surface changing the local refractive index and the reflection angle. The increase in the reflection

angle is measured as the sensorgram change for quantitative analysis (Figure 1C, see detailed information in Supporting Information). Similar experiments were also carried out with functionalized MCL sensors with repeated injections with DA. The displacement of P($LAEMA_{21}$) by DA results in surface stress variation, which causes the microcantilever to bend (Figure 1D).

Figure 2 shows the experimental arrangement and the results for DA detection using cantilever arrays. A microcantilever array with 8 cantilevers was functionalized using capillary tubes, where the Group I was functionalized with P($NIPAAm_{149}$-*st*-$MAAmBO_{19}$) only and the group III was functionalized with conjugated P($NIPAAm_{149}$-*st*-$MAAmBO_{19}$) and P($LAEMA_{21}$). The cantilevers in the Group II were functionalized with PEG and served as reference cantilevers. The functionalized MCL array was mounted in a flowcell with a constant PBS flow of 5 mL h^{-1}. DA sample with a concentration of 5 nM was injected into the flow without changing the flow rate, followed by PBS rinsing. As shown in Figure 2B, the PEG functionalized group had negligible responses to DA injection while the bending signal of other groups of microcantilevers built up over time. After about 3000 seconds, the bending of the conjugated polymer and P($NIPAAm_{149}$-*st*-$MAAmBO_{19}$) functionalized microcantilevers reached a steady state of about 95 nm and 140 nm (correspond to surface stress differential of 27 mN m^{-1} and 40 mN m^{-1}) respectively. An increase in the deflection indicates an increase in the surface stress on the polymer functionalized surface, which suggests the DA binding swells the polymers[24,25]. However, deflection change of the conjugated P($NIPAAm_{149}$-*st*-$MAAmBO_{19}$) and P($LAEMA_{21}$) functionalized cantilevers is slightly less than that of P($NIPAAm_{149}$-*st*-$MAAmBO_{19}$) functionalized ones. This is possibly due to the pre-conjugated P($LAEMA_{21}$) swelling the P($NIPAAm_{149}$-*st*-$MAAmBO_{19}$) before the DA was injected. Thus, when the DA displaced the P($LAEMA_{21}$), the swelling effect was less intense. Since the binding affinity between P($NIPAAm_{149}$-*st*-$MAAmBO_{19}$) and P($LAEMA_{21}$) is a critical factor

for achieving enhanced selectivity of the sensor, slightly reduced sensitivity (due to reduced swelling) is acceptable.

The sensitivity and the limit of detection (LOD) of the polymer assisted MCL sensors were determined by injecting DA samples with various concentrations following the similar protocol described above. Freshly functionalized MCL sensors were used for each DA sample injections. From Figure 2C, it is clear that as DA concentration increased from 50 pM to 50 nM, microcantilever deflection change increased from 15 nm to 240 nm. Since the average noise level was ~5 nm, the LOD (for S/N≈3) of microcantilever sensor can be estimated as two orders of magnitude lower than the physiologically relevant level[11]. The P(NIPAAm$_{149}$-*st*-MAAmBO$_{19}$) swelling is enhanced with increasing DA concentration. A typical detection time for the MCL sensor is 5000 seconds under the test condition, which can be further adjusted by applying different flow rates. Figure 2D shows the variation of adsorption rate (*k)* as a function of different DA concentrations. For DA concentration increase from 50 pM to 5 nM, the adsorption rate showed an increase from 0.3×10^{-3} s^{-1} to 1.1×10^{-3} s^{-1}. This increase in the adsorption rate may be due to the availability of the multiple oxaborole units in the P(NIPAAm$_{149}$-*st*-MAAmBO$_{19}$) polymer chain as binding sites. However, for 50 nM DA injection, the adsorption rate decreases, which may be due to the saturation of the binding sites on the microcantilever surface.

Figure 3 shows the sensitivity and dynamic range of the functionalized SPR sensor. Since the lowest DA concentration in physiological samples is around 10^{-9} M (1 nM), the sensitivity and resolution of the polymer functionalized SPR sensor was determined at nanomolar range. The injection of 1 nM DA generated 5.3 millidegree increase in sensorgram and the equilibrium was reached at about 800 seconds after injection. The sensorgram evolution with the DA concentration is demonstrated in Figure 3A. For each DA sample injection from 1 to 10 nM, the corresponding sensorgram change is 5 millidegree

(S/N≈5). The relation between the DA concentration (1 to 10 nM) and the sensorgram change is shown in Figure 3B. Thus, from 1 to 10 nM, the sensorgram exhibits a linear relation with DA concentration with a LOD of 1 nM.

The DA adsorption rate (*k*) also varies with the DA concentration. As the concentration changes from 1 to 10 nM, the adsorption rate (*k)* increases from 1.1×10^{-3} s^{-1} to 6.5×10^{-3} s^{-1} (Figure 3C). As indicated previously, the increased adsorption rate with increasing DA concentration can be due to the availability of the multiple binding sites on the P(NIPAAm$_{149}$-*st*-MAAmBO$_{19}$) chain. Interestingly, the adsorption rate of the SPR sensor is higher than that of the microcantilever sensor, which leads to a reduced detection time. The increasing adsorption rate for 1 to 10 nM of DA also suggests that the DA concentration can be measured accurately in this range.

The dynamic range of the polymer functionalized SPR sensor was determined by injecting DA samples from 10^{-9} to 10^{-4} M. As shown in Figure 3D, the sensorgram increases up to 300 times from 5 millidegrees to over 1.3 degrees while the DA concentration increases five orders of magnitude. It demonstrates that the polymer functionalized SPR sensor has a broad working range for DA detection. In contrast, the sensorgram of PEG functionalized blank reference chip does not change significantly with DA concentration. However, with higher DA concentration, the resolution of the conjugated polymer functionalized sensor decreases as shown in Figure 3D. The decrease in resolution can be attributed to the saturation of the binding sites. DA binds onto the sensor surface through a displacement reaction with pre-conjugated P(LAEMA$_{21}$). However, the conjugated DA will affect the orientation of P(NIPAAm$_{149}$-*st*-MAAmBO$_{19}$) which leads to the inhibition of the further DA adsorption. Also, when the injected DA samples are concentrated enough, there are not enough binding sites for the excess DA molecules; thus the sensor resolution decreases.

The capability of distinguishing the target analyte of clinical samples is usually the major challenge for developing biosensors. The selectivity of the conjugated polymer sensing layer was investigated by comparing sensorgram variation caused by different injections with 5 nM DA, glucose, AA and UA samples using SPR sensors functionalized with conjugated P(NIPAAm$_{149}$-*st*-MAAmBO$_{19}$) and P(LAEMA$_{21}$); P(NIPAAm$_{149}$-*st*-MAAmBO$_{19}$) only and PEG as blank control. Recognition tests were performed using EPI, AA and UA as the structural analogs and different monosaccharides (glucose, fructose, and mannose) as other potential co-existing molecules with diols of equal or higher concentrations of 5, 50 and 500 nM.

The selectivity of the sensor was attributed by the conjugated P(NIPAAm$_{149}$-*st*-MAAmBO$_{19}$) and P(LAEMA$_{21}$) layer as stated previously. As demonstrated in Figure 4A, PEG functionalized sensor was almost inert to any sample injections. The P(NIPAAm$_{149}$-*st*-MAAmBO$_{19}$) showed significant response to 5 nM DA injection and a much lower response to AA or UA injections, but it failed to distinguish the glucose sample from DA. In contrast, the conjugated polymer layer has little response to glucose injection due to the estimated higher binding constant between P(NIPAAm$_{149}$-*st*-MAAmBO$_{19}$) and P(LAEMA$_{21}$) than that between P(NIPAAm$_{149}$-*st*-MAAmBO$_{19}$) and glucose. On average, one P(LAEMA$_{21}$) molecule has two cis-diol units on the each side chain which lead to a higher binding constant to P(NIPAAm$_{149}$-*st*-MAAmBO$_{19}$) than that of glucose. According to previous studies of binding constant[15], the maximum estimated binding constant is lower than that of DA. As compared to molecules with aliphatic hydroxyls, the aromatic hydroxyls from DA molecules can form more stable cyclic-esters with oxaborole groups. In addition, the aromatic groups in DA can further stabilize the cyclic-ester structure. Thus, the conjugated polymer functionalized sensor is selective to DA only. However, the conjugated polymers and P(NIPAAm$_{149}$-*st*-MAAmBO$_{19}$) functionalized SPR chips showed similar response with 5 nM DA sample, which is due to the similar level of thickness and

surface roughness change caused by DA binding. This effect was further confirmed by AFM topography and surface roughness study. In addition, 5 nM DA did not saturate the SPR sensor surface, which also lead to similar sensorgram response.

It can be found in Figure 4B that sensorgram of DA slightly increases with the added saccharides. Fructose, which has the highest binding constant (~4000 K mol^{-1}) to boronic groups among the monosaccharides[15], introduced the largest sensorgram increase of about 11% when 500 nM of fructose was added. Due to the fact that the conjugated P($LAEMA_{21}$) has a higher binding affinity than the free monosaccharides, the displacement reaction happens when DA presented. Thus, the conjugated polymer functionalized sensor is capable of recognizing DA with coexisting saccharides. As illustrated in Figure 4C, the coexisting compounds UA and AA do not affect the detection at 100 times higher concentration than that of DA in the injected sample mixtures. This demonstrates that the sensor is highly selective to DA over UA or AA. However, with 10 times and 100 times concentrated EPI mixed in DA samples, the sensorgram level increased to about 15% and 40%. This effect of EPI was due to the structural similarity of the DA and EPI. Both molecules belong to catecholamine family (with catechol groups), which make them able to form covalent bonds with oxaborole groups on P($NIPAAm_{149}$-*st*-$MAAmBO_{19}$) and displace P($LAEMA_{21}$) from the conjugated polymer. It can be inferred that other molecules in catecholamine family (e.g. norepinephrine, NE) or large molecules (e.g. glycoproteins) can also interfere the detection results. Yet, comparing with other DA sensors[10,11], this polymer functionalized SPR sensor has demonstrated high DA selectivity at nanomolar range.

The mechanism of signal generation, changes in surface stress and refractive index, is attributed to DA binding induced swelling. We have carried out ^{11}B NMR to characterize the DA displacement reaction. Previous studies of ^{11}B NMR showed the ^{11}B chemical shift peak move to lower field when electron-

withdrawing groups bound to boronic acid[26]. As illustrated in Figure S1, P(NIPAAm$_{149}$-*st*-MAAmBO$_{19}$) revealed a single ^{11}B peak at 19.5 ppm. Upon addition of P(LAEMA$_{21}$) to the solution, two small peaks at 10.9 ppm and 10.5 ppm were observed, indicating the binding between P(NIPAAm$_{149}$-*st*-MAAmBO$_{19}$) and P(LAEMA$_{21}$). Furthermore, when DA was added into the solution, the two peaks at 10.5 and 10.9 ppm disappeared and a new signal peak was observed at 7.9 ppm, which indicated the binding of DA to P(NIPAAm$_{149}$-*st*-MAAmBO$_{19}$) by displacing P(LAEMA$_{21}$). In comparison to the P(LAEMA$_{21}$), DA, with a catechol group and its aromatic nature, shifted the ^{11}B peak to the lower field. It can be inferred that oxaborole group forms a far more stable cyclic-ester with the catechol group than with oriented cis-diols. Thus, DA can displace the conjugated P(LAEMA$_{21}$) while the other compounds like saccharides, AA and UA can only bind to a minimum extent.

We have also used AFM for characterizing the changes in the surface morphology of polymer layer due to DA adsorption. A FastScan C probe with a spring constant of 0.8 N m^{-1} was used for imaging. From comparing the topography of an SPR chip before and after conjugated polymer immobilization (Figure S2A and S2B), it can be concluded that during immobilization, irregularly shaped aggregates of 20 nm thickness formed on the gold-coated SPR sensor chip. Figure S2C shows that, after the 5 nM DA injection, the polymer layer thickness increased to 25 nm, indicating the swelling of P(NIPAAm$_{149}$-*st*-MAAmBO$_{19}$) due to DA binding. Also, the surface roughness increases from 4.8 to 5.2 nm after the DA displaced the P(LAEMA$_{21}$), which is also due to the swelling after DA binding. The 25 % swelling of the polymer layer thickness increases the local refractive index. In addition, the swelling of P(NIPAAm$_{149}$-*st*-MAAmBO$_{19}$) enhances the interaction between gold surface and PBS medium, resulting in an increase in the local refractive index. As a result, SPR sensorgram shifts due to DA binding to P(NIPAAm$_{149}$-*st*-MAAmBO$_{19}$) and resultant displacement of P(LAEMA$_{21}$). In contrast, the SPR chip with only P(NIPAAm$_{149}$-*st*-MAAmBO$_{19}$) yields a 28-nm-thick polymer layer, and after DA

binding it increases to about 35 nm with a roughness increase from 5.5 to 6.8 nm (Figure S2D and S2E). Both polymer functionalized sensing layer has a comparable thickness with typical synaptic cleft distance (20-40 nm)[27], which makes it ideal for DA fast-scan detection. This result also confirms the previous selectivity test such that, with only P(NIPAAm$_{149}$-*st*-MAAmBO$_{19}$) on the surface, the initial polymer thickness and roughness are larger than that with conjugated polymers indicating the binding of P(LAEMA$_{21}$) increased the total coverage on the gold surface. On the other hand, the thickness and roughness variation of the conjugated polymer is less than that of the P(NIPAAm$_{149}$-*st*-MAAmBO$_{19}$) but only slightly. Thus, the SPR sensorgram response from the conjugated polymer functionalized chip is lower than that of P(NIPAAm$_{149}$-*st*-MAAmBO$_{19}$) functionalized one.

Compared with previously reported DA detection methods, the conjugated polymer functionalized MCL and SPR sensors have at least one order of magnitude improvement in LOD for DA detection[28,29]. In addition, the conjugated polymer functionalized sensors also have a relatively simpler preparation procedure without incorporating enzymes or other bio-componants[9,30]. The high sensitivity and selectivity of the presented sensor systems are due to the combined advantages of optimum binding affinity between P(LAEMA$_{21}$) and P(NIPAAm$_{149}$-*st*-MAAmBO$_{19}$), the DA displacement binding reaction, and the sensitivity of MCL and SPR sensor platforms. Compared to MCL sensor results, the SPR sensor does not achieve sub-nanomolar detection limit. However, the measured LOD at the nanomolar range is ideal for clinical detection. With the sensors as tested, the SPR sensor shows much-reduced detection time than the MCL sensor which is an advantage in potential clinical applications. Compared with other DA detection methods[31], the conjugated polymer system offers a much simplified and compact sensor setup. Also, with a much faster detection and in real-time, in-line detection is possible. Usually, surface functionalization is one of the major limits for most of the surface related sensing techniques. However, this conjugated polymer system synthesized by RAFT method allowed

the easy formation of self-assembled layer on gold coated sensor surface via the Au-thiol interactions. As shown by both MCL and SPR sensors, this conjugated polymer system can potentially be used in other sensor platforms.

In this study, we also take the advantage of the reversible covalent interaction between diols and oxaborole groups to design potential reusable biosensors. A surface regeneration procedure was performed by washing with pH 4 PBS, and followed by the re-conjugation of P($LAEMA_{21}$)[14,17]. The sensor regeneration was tested over 5 times and evaluated using 5 nM DA sample. The sensorgram signal showed less than 10% decrease after 5 regeneration cycles, but it still showed reliable and reproducible results (Figure 5A).

The sensor stability was also evaluated for over 2 weeks under ambient condition. From day 1 to 15, the sensorgram change representing 5 nM DA injections decreased about 10% (Figure 5B). It can be concluded that the polymer functionalized sensor is stable for at least 2 weeks. Comparing with methods using specific DA receptors[9], the conjugated polymer system provides much improved stability.

In summary, a conjugated polymer layer consisting of P($NIPAAm_{149}$-*st*-$MAAmBO_{19}$) and P($LAEMA_{21}$) was designed for real-time detection of dopamine with high selectivity, sensitivity and broad dynamic range. Sensing performance of the conjugated polymer was evaluated using MCL and SPR sensor platforms. The SPR sensor achieved a fast response time and a wide dynamic range from 10^{-9} to 10^{-4} M with a limit of detection of 1 nM, while the LOD for the MCL was 50 pM. Due to the optimum binding affinity between P($NIPAAm_{149}$-*st*-$MAAmBO_{19}$) and P($LAEMA_{21}$), this conjugated polymer sensing layer showed high selectivity to dopamine but little cross-reactivity to coexisting compounds like

ascorbic acid, uric acid and saccharides. In addition, the sensing layer could be regenerated and reused for multiple times and was stable over 2 weeks at ambient conditions. Future studies will focus on real clinical sample selectivity and reliability test. This conjugated polymer system could be exploited as a unique method for DA detection clinically.

ASSOCIATED CONTENT

Supporting Information

The Supporting Information is available free of charge on the ACS Publications website.

Detection mechanisms of SPR and MCL sensor platforms, Materials and Instrumentation, Surface functionalization procedure and AFM and NMR characterization, detailed experimental procedures. (PDF)

AUTHOR INFORMATION

Corresponding Author

Emails: narain@ualberta.ca (R.N.), thundat@ualberta.ca (T.T.)

Notes

The authors declare no competing financial interests.

ACKNOWLEDGMENTS

This work was supported by Canada Excellent Research Chair (CERC). K. J. was a recipient of Alberta Innovates Technology Futures (AITF) Graduate Scholarship. We would like to thank Dr. Vishwa Somayaji for the assistance of NMR characterization.

REFERENCES

(1) Gonon, F.; Buda, M.; Cespuglio, R.; Jouvet, M.; Pujol, J.F. In Vivo Electrochemical Detection of Catechols in the Neostriatum of Anaesthetized Rats: Dopamine or DOPAC? *Nature* **1980**, *286* (5776), 902–904.

(2) Keefe, K. A.; Zigmond, M. J.; Abercrombie, E. D. In Vivo Regulation of Extracellular Dopamine in the Neostriatum: Influence of Impulse Activity and Local Excitatory Amino Acids. *J. Neural Transm. Gen. Sect.* **1993**, *91* (2–3), 223–240.

(3) Clark, J. J.; Sandberg, S. G.; Wanat, M. J.; Gan, J. O.; Horne, E. A.; Hart, A. S.; Akers, C. A.; Parker, J. G.; Willuhn, I.; Martinez, V.; Evans, S. B.; Stella, N.; Phillips, P. E. M. Chronic Microsensors for Longitudinal, Subsecond Dopamine Detection in Behaving Animals. *Nat. Methods* **2010**, *7* (2), 126–129.

(4) Rao, P. S.; Rujikarn, N.; Luber, J. M.; Tyras, D. H. A Specific Sensitive HPLC Method for Determination of Plasma Dopamine. *Chromatographia* **1989**, *28* (5–6), 307–310.

(5) Woolley, A. T.; Lao, K.; Glazer, A. N.; Mathies, R. A. Capillary Electrophoresis Chips with Integrated Electrochemical Detection. *Anal. Chem.* **1998**, *70* (4), 684–688.

(6) Fotopoulou, M. A.; Ioannou, P. C. Post-Column Terbium Complexation and Sensitized Fluorescence Detection for the Determination of Norepinephrine, Epinephrine and Dopamine Using High-Performance Liquid Chromatography. *Anal. Chim. Acta* **2002**, *462* (2), 179–185.

(7) Khan, A. F.; Brownson, D. A. C.; Randviir, E. P.; Smith, G. C.; Banks, C. E. 2D Hexagonal Boron Nitride (2D-hBN) Explored for the Electrochemical Sensing of Dopamine. *Anal. Chem.* **2016**, *88* (19), 9729–9737.

(8) Qi, L.; Thomas, E.; White, S. H.; Smith, S. K.; Lee, C. A.; Wilson, L. R.; Sombers, L. A. Unmasking the Effects of L-DOPA on Rapid Dopamine Signaling with an Improved Approach for Nafion Coating Carbon-Fiber Microelectrodes. *Anal. Chem.* **2016**, *88* (16), 8129–8136.

(9) Park, S. J.; Lee, S. H.; Yang, H.; Park, C. S.; Lee, C.S.; Kwon, O. S.; Park, T. H.; Jang, J. Human Dopamine Receptor-Conjugated Multidimensional Conducting Polymer Nanofiber Membrane for Dopamine Detection. *ACS Appl. Mater. Interfaces* **2016**, *8* (42), 28897–28903.

(10) Zeng, Z.; Cui, B.; Wang, Y.; Sun, C.; Zhao, X.; Cui, H. Dual Reaction-Based Multimodal Assay for Dopamine with High Sensitivity and Selectivity Using Functionalized Gold Nanoparticles. *ACS Appl. Mater. Interfaces* **2015**, *7* (30), 16518–16524.

(11) Chen, C.H.; Luo, S.C. Tuning Surface Charge and Morphology for the Efficient Detection of Dopamine under the Interferences of Uric Acid, Ascorbic Acid, and Protein Adsorption. *ACS Appl. Mater. Interfaces* **2015**, *7* (39), 21931–21938.

(12) Guo, Z.; Seol, M.L.; Kim, M.S.; Ahn, J.H.; Choi, Y.K.; Liu, J.H.; Huang, X.J. Sensitive and Selective Electrochemical Detection of Dopamine Using an Electrode Modified with Carboxylated Carbonaceous Spheres. *Analyst* **2013**, *138* (9), 2683–2690.

(13) Lacina, K.; Skládal, P.; James, T. D. Boronic Acids for Sensing and Other Applications - a Mini-Review of Papers Published in 2013. *Chem. Cent. J.* **2014**, 8 (1), 60.

(14) Kotsuchibashi, Y.; Agustin, R. V. C.; Lu, J.Y.; Hall, D. G.; Narain, R. Temperature, pH, and Glucose Responsive Gels via Simple Mixing of Boroxole- and Glyco-Based Polymers. *ACS Macro Lett.* **2013**, *2* (3), 260–264.

(15) James, T. D.; Phillips, M. D.; Shinkai, S. *Boronic Acids in Saccharide Recognition*; Royal Society of Chemistry: Cambridge, UK, 2006.

(16) Floresco, S. B.; West, A. R.; Ash, B.; Moore, H.; Grace, A. A. Afferent Modulation of Dopamine Neuron Firing Differentially Regulates Tonic and Phasic Dopamine Transmission. *Nat. Neurosci.* **2003**, *6* (9), 968–973.

(17) Wang, Y.; Kotsuchibashi, Y.; Uto, K.; Ebara, M.; Aoyagi, T.; Liu, Y.; Narain, R. pH and Glucose Responsive Nanofibers for the Reversible Capture and Release of Lectins. *Biomater. Sci.* **2015**, *3* (1), 152–162.
(18) Pattnaik, P. Surface Plasmon Resonance. *Appl. Biochem. Biotechnol.* **2005**, *126* (2), 79–92.
(19) Matsui, J.; Akamatsu, K.; Hara, N.; Miyoshi, D.; Nawafune, H.; Tamaki, K.; Sugimoto, N. SPR Sensor Chip for Detection of Small Molecules Using Molecularly Imprinted Polymer with Embedded Gold Nanoparticles. *Anal. Chem.* **2005**, *77* (13), 4282–4285.
(20) Hansen, K. M.; Thundat, T. Microcantilever Biosensors. *Methods* **2005**, *37* (1), 57–64.
(21) Anker, J. N.; Hall, W. P.; Lyandres, O.; Shah, N. C.; Jing Zhao; Van Duyne, R. P. Biosensing with Plasmonic Nanosensors. *Nat. Mater.* **2008**, *7* (6), 442–453.
(22) Datar, R.; Kim, S.; Jeon, S.; Hesketh, P.; Manalis, S.; Boisen, A.; Thundat, T. Cantilever Sensors: Nanomechanical Tools for Diagnostics. *MRS Bull.* **2009**, *34* (6), 449–454.
(23) Azmi, S.; Jiang, K.; Stiles, M.; Thundat, T.; Kaur, K. Detection of Listeria Monocytogenes with Short Peptide Fragments from Class IIa Bacteriocins as Recognition Elements. *ACS Comb. Sci.* **2015**, *17* (3), 156–163.
(24) Pei, J.; Tian, F.; Thundat, T. Glucose Biosensor Based on the Microcantilever. *Anal. Chem.* **2004**, *76* (2), 292–297.
(25) Matsumoto, A.; Ikeda, S.; Harada, A.; Kataoka, K. Glucose-Responsive Polymer Bearing a Novel Phenylborate Derivative as a Glucose-Sensing Moiety Operating at Physiological pH Conditions. *Biomacromolecules* **2003**, *4* (5), 1410–1416.
(26) Baldwin, J. E.; Claridge, T. D. W.; Derome, A. E.; Schofield, C. J.; Smith, B. D. ^{11}B NMR Studies of an Aryl Boronic Acid Bound to Chymotrypsin and Subtilisin. *Bioorg. Med. Chem. Lett.* **1991**, *1* (1), 9–12.
(27) Kandel, E. R.; Schwartz, J. H.; Jessell, T. M.; Siegelbaum, S. A.; Hudspeth, A. J. *Principles of Neural Science, 5th ed*; McGraw Hill: New York, 2012.
(28) Stewart, A. J.; Hendry, J.; Dennany, L. Whole Blood Electrochemiluminescent Detection of Dopamine. *Anal. Chem.* **2015**, *87* (23), 11847–11853.
(29) Yang, C.; Jacobs, C. B.; Nguyen, M. D.; Ganesana, M.; Zestos, A. G.; Ivanov, I. N.; Puretzky, A. A.; Rouleau, C. M.; Geohegan, D. B.; Venton, B. J. Carbon Nanotubes Grown on Metal Microelectrodes for the Detection of Dopamine. *Anal. Chem.* **2016**, *88* (1), 645–652.
(30) Njagi, J.; Chernov, M. M.; Leiter, J. C.; Andreescu, S. Amperometric Detection of Dopamine in Vivo with an Enzyme Based Carbon Fiber Microbiosensor. *Anal. Chem.* **2010**, *82* (3), 989–996.
(31) Feng, J.J.; Guo, H.; Li, Y.F.; Wang, Y.H.; Chen, W.Y.; Wang, A.J. Single Molecular Functionalized Gold Nanoparticles for Hydrogen-Bonding Recognition and Colorimetric Detection of Dopamine with High Sensitivity and Selectivity. *ACS Appl. Mater. Interfaces* **2013**, *5* (4), 1226–1231.

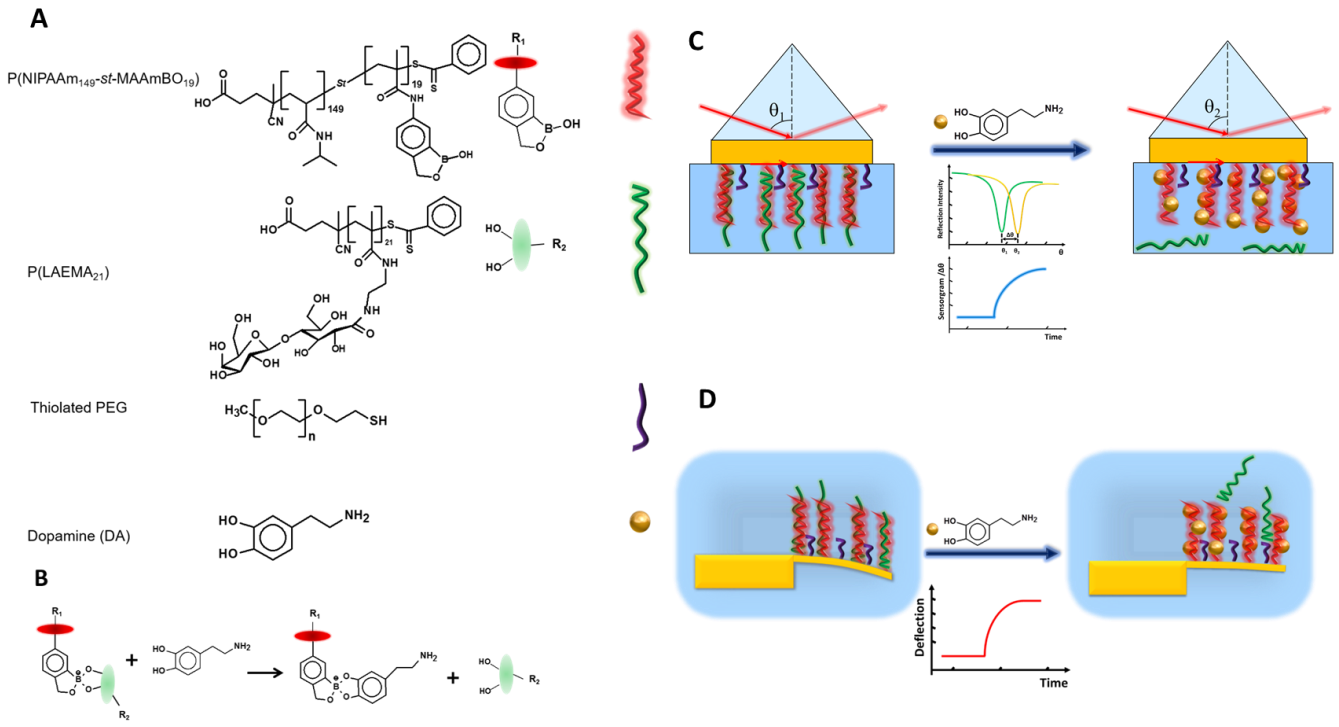

Figure 1. Polymer structures, binding of dopamine to oxaborole residues, SPR and MCL sensor platforms. A: Structures of the P(NIPAAm$_{149}$-*st*-MAAmBO$_{19}$), P(LAEMA$_{21}$) and DA; B: a brief equation showing the adsorption-displacement reaction on the sensor surface; C: Schematics illustrating light reflection angle change due to the surface plasmon resonance change caused by selective adsorption of molecules on gold surface; D: microcantilever deflection change due to DA displacement on conjugated polymer surface.

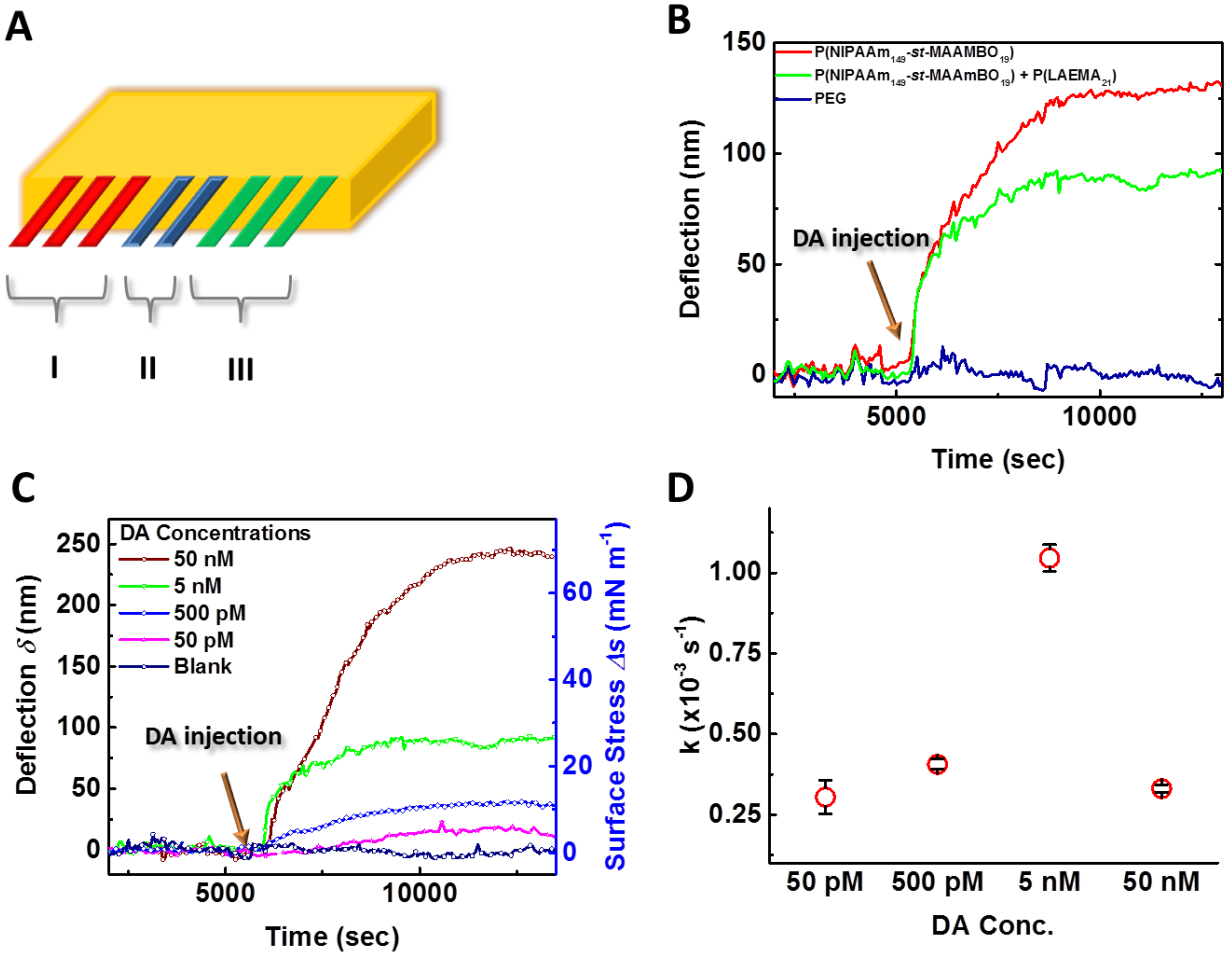

Figure 2. Microcantilever sensor array was used to monitor the polymer swelling with DA binding. A: schematic showing the MCL array functionalized with 3 different polymer layers, I: P(NIPAAm$_{149}$-*st*-MAAmBO$_{19}$) layer; II: PEG layer as blank reference; III: P(NIPAAm$_{149}$-*st*-MAAmBO$_{19}$) and P(LAEMA$_{21}$) conjugated layer; B: MCL bending with 5 nM DA injection: P(NIPAAm$_{149}$-*st*-MAAmBO$_{19}$) and P(LAEMA$_{21}$) functionalized microcantilevers have an average bending of 95 nm while P(NIPAAm$_{149}$-*st*-MAAmBO$_{19}$) functionalized beams bend 140 nm, indicating a larger amount of swelling. However, the binding affinity between P(NIPAAm$_{149}$-*st*-MAAmBO$_{19}$) and P(LAEMA$_{21}$) is one crucial factor of the sensor selectivity; C: MCL bending deflection increase with injected DA concentration from 50 pM to 50 nM from 15 nm to 240 nm; D: the binding constant (k) increases from 50 pM to 5 nM indicating a faster displacement reaction with increased DA concentrations, but a decrease of 50 nM sample suggests the saturation of the sensor surface.

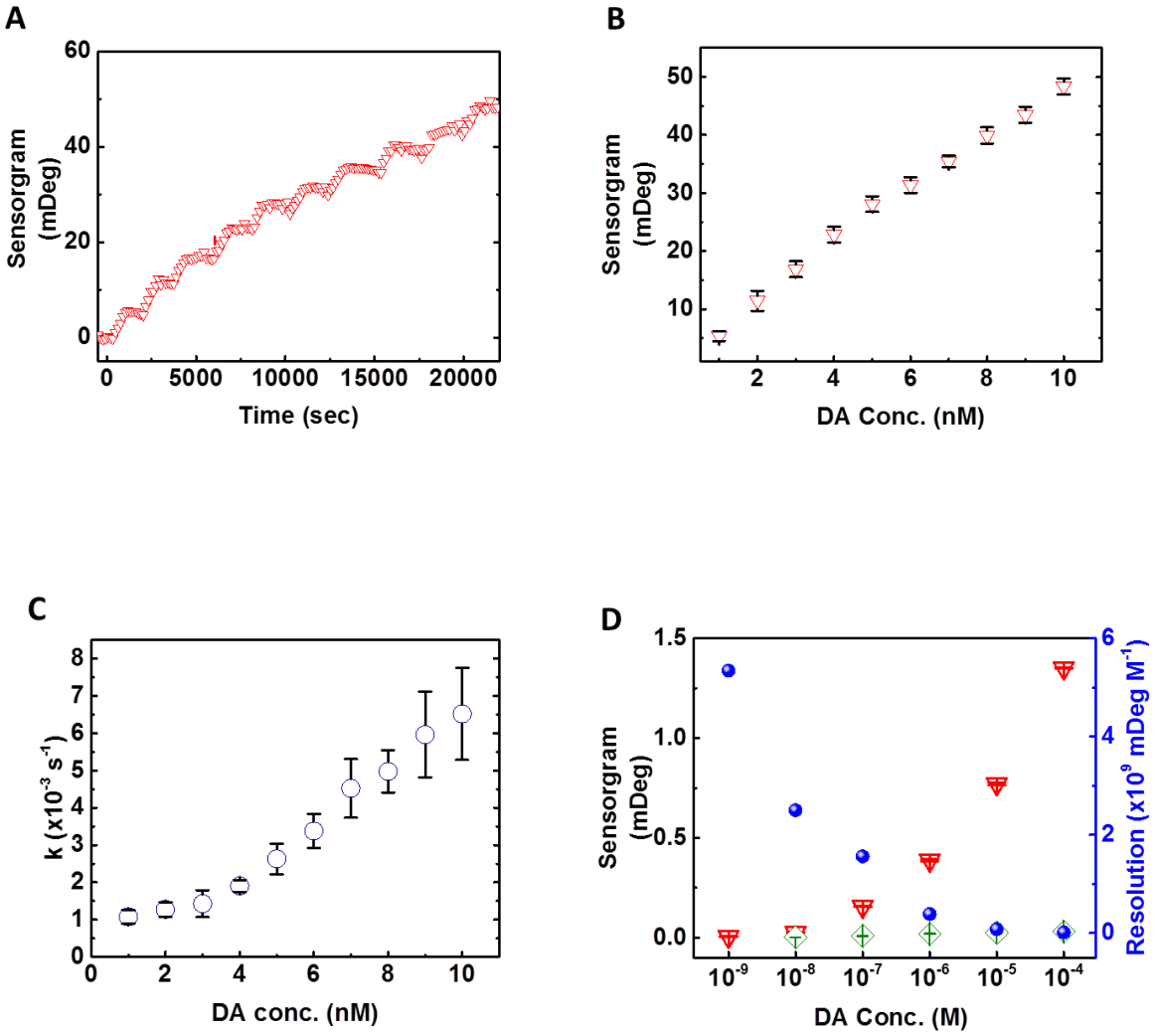

Figure 3. Sensitivity and working range of the P(NIPAAm$_{149}$-*st*-MAAmBO$_{19}$) and P(LAEMA$_{21}$) functionalized SPR sensor. A: SPR sensorgram increase from 5 to 50 millidegree with DA concentration from 1 to 10 nM; B: from 1 to 10 nM, the sensorgram-concentration presented a linear relationship; C: the DA adsorption rate increase from 1 to 10 nM due to the reaction kinetics; D: SPR sensorgram increase from 0.005° to ~1.4° over 5 folds of DA concentration with the conjugated polymer functionalized sensor(red) while the sensorgram remained identical with PEG functionalized sensor(green); and resolution of the functionalized SPR sensor decrease with the DA concentration.

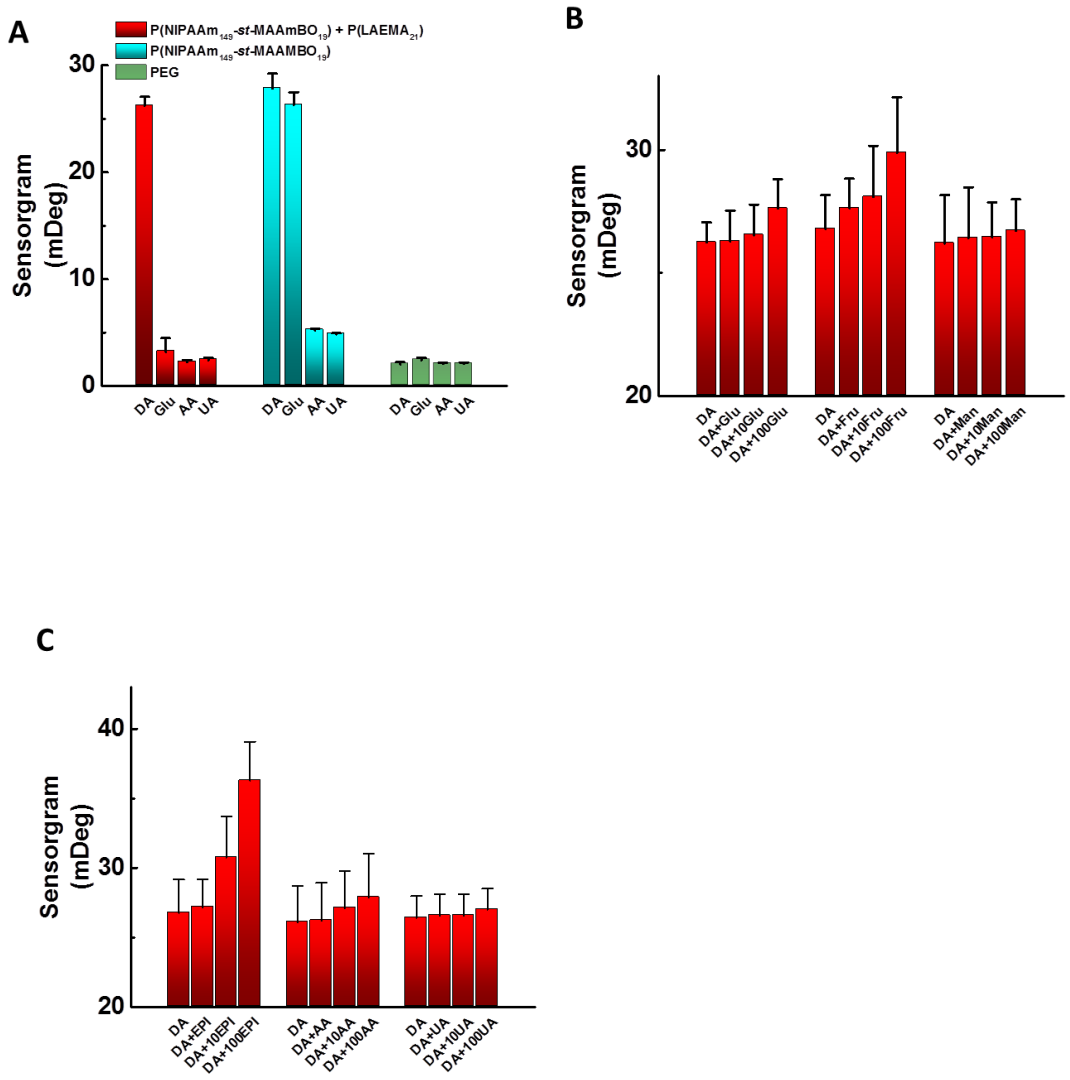

Figure 4. Selectivity and recognition test for the polymer assisted SPR sensor. A: selectivity of polymer sensing layer: with P(NIPAAm$_{149}$-*st*-MAAmBO$_{19}$) and P(LAEMA$_{21}$) functionalization, the sensor is selective to DA only; with only P(NIPAAm$_{149}$-*st*-MAAmBO$_{19}$), the sensing layer does not show any selectivity to DA; B: DA with monosaccharides; C: DA with other potential co-existed molecules and structural analogs. The functionalized polymer assay showed higher affinity toward DA than the saccharides, AA and UA, however, EPI interfered the sensorgram due to the structural similarity. All the tests are based on DA concentration of 5 nM.

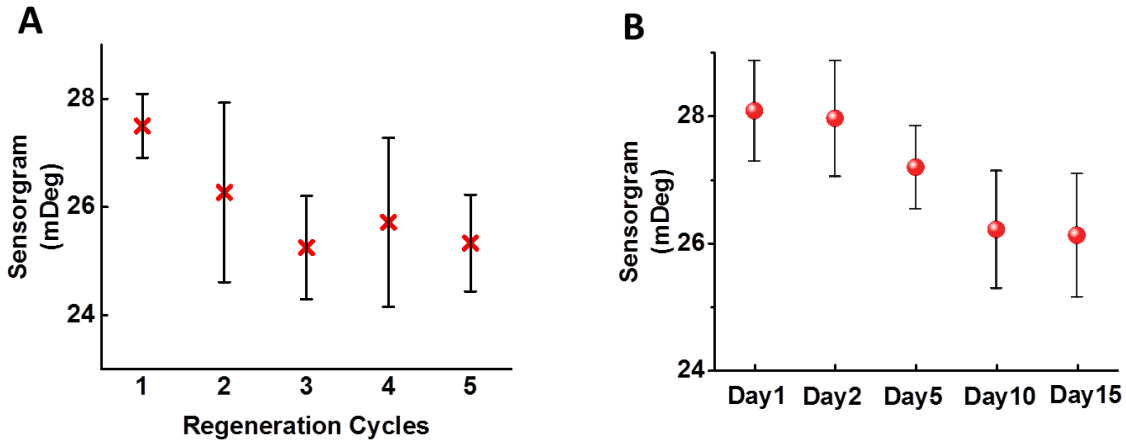

Figure 5. Sensor regeneration and stability test with 5 nM DA injections. A: SPR sensorgram signal reduced less than 10% after 5 times regeneration; B: the functionalized sensor remained 95% sensorgram signal within 5 days after surface functionalization and 90% after 15 days.

TOC

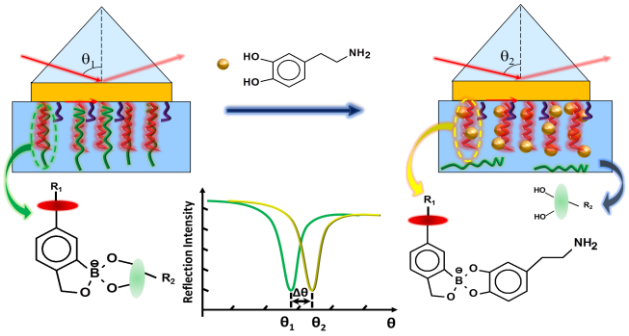

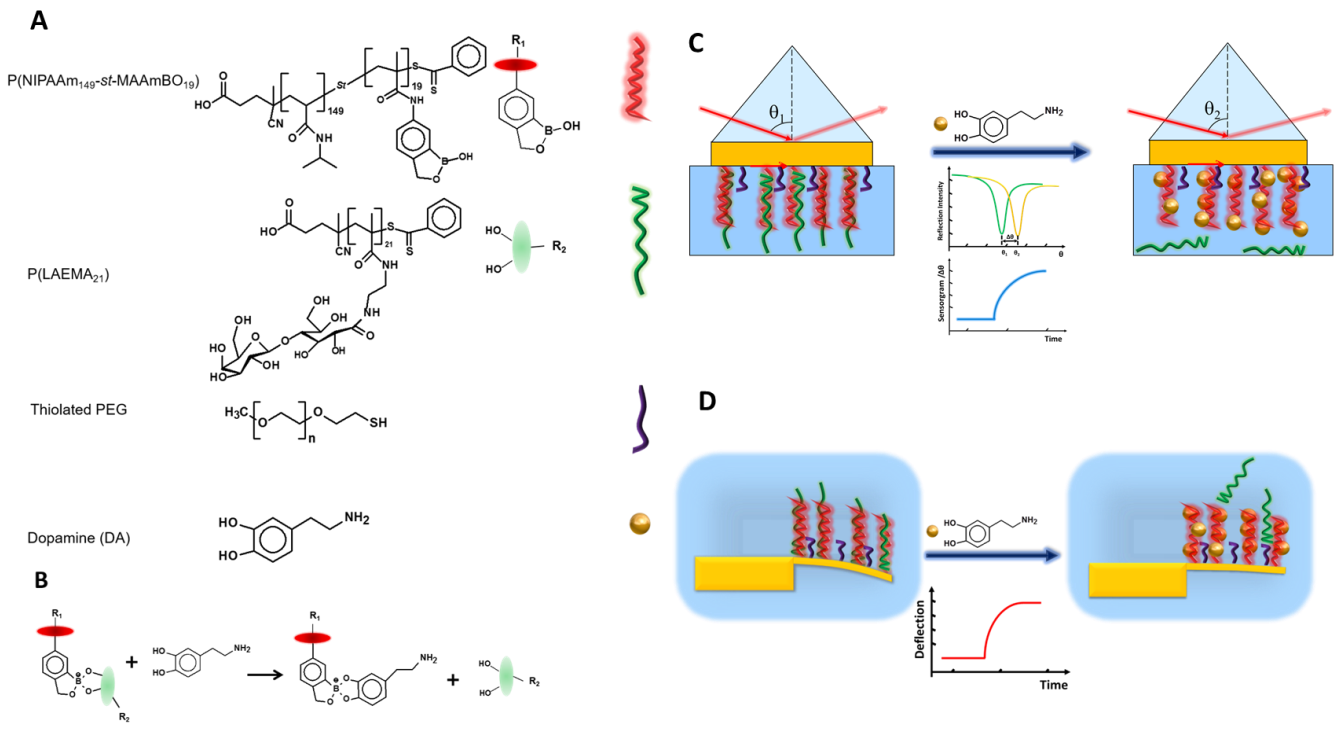

Figure 1. Polymer structures, binding of dopamine to oxaborole residues, SPR and MCL sensor platforms. A: Structures of the P(NIPAAm$_{149}$-*st*-MAAmBO$_{19}$), P(LAEMA$_{21}$) and DA; B: a brief equation showing the adsorption-displacement reaction on the sensor surface; C: Schematics illustrating light reflection angle change due to the surface plasmon resonance change caused by selective adsorption of molecules on gold surface; D: microcantilever deflection change due to DA displacement on conjugated polymer surface.

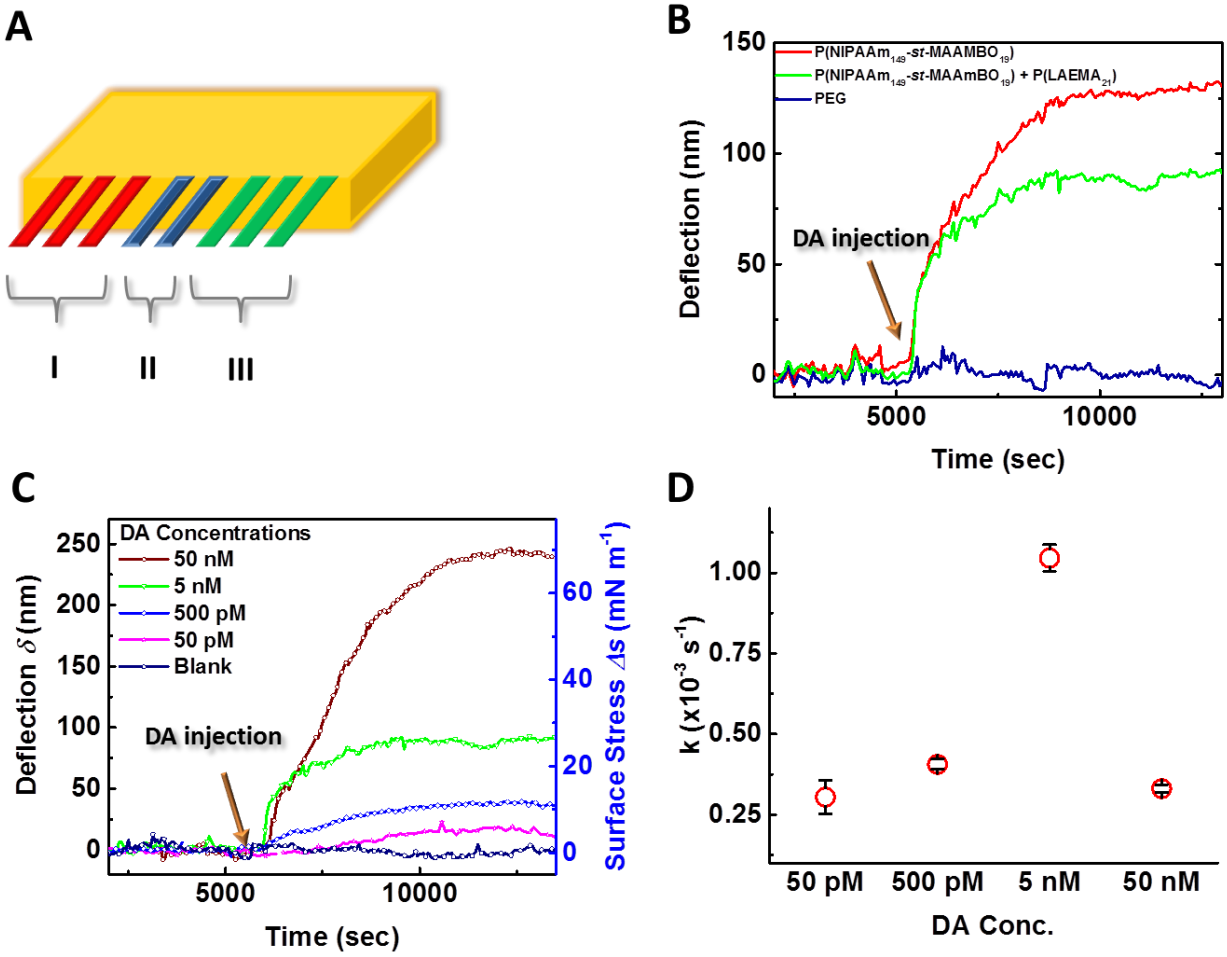

Figure 2. Microcantilever sensor array was used to monitor the polymer swelling with DA binding. A: schematic showing the MCL array functionalized with 3 different polymer layers, I: P(NIPAAm$_{149}$-*st*-MAAmBO$_{19}$) layer; II: PEG layer as blank reference; III: P(NIPAAm$_{149}$-*st*-MAAmBO$_{19}$) and P(LAEMA$_{21}$) conjugated layer; B: MCL bending with 5 nM DA injection: P(NIPAAm$_{149}$-*st*-MAAmBO$_{19}$) and P(LAEMA$_{21}$) functionalized microcantilevers have an average bending of 95 nm while P(NIPAAm$_{149}$-*st*-MAAmBO$_{19}$) functionalized beams bend 140 nm, indicating a larger amount of swelling. However, the binding affinity between P(NIPAAm$_{149}$-*st*-MAAmBO$_{19}$) and P(LAEMA$_{21}$) is one crucial factor of the sensor selectivity; C: MCL bending deflection increase with injected DA concentration from 50 pM to 50 nM from 15 nm to 240 nm; D: the binding constant (k) increases from 50 pM to 5 nM indicating a faster displacement reaction with increased DA concentrations, but a decrease of 50 nM sample suggests the saturation of the sensor surface.

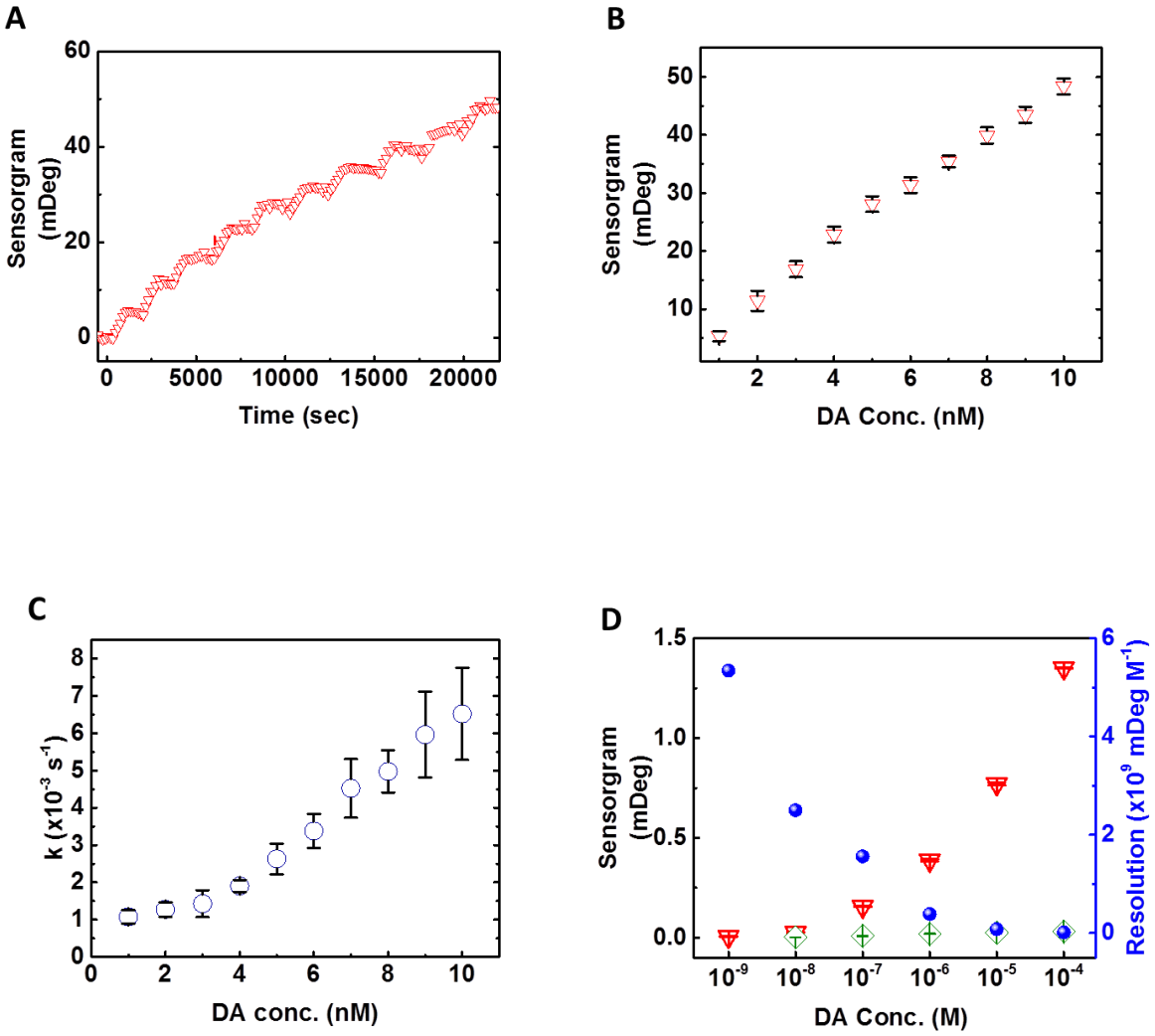

Figure 3. Sensitivity and working range of the P(NIPAAm$_{149}$-*st*-MAAmBO$_{19}$) and P(LAEMA$_{21}$) functionalized SPR sensor. A: SPR sensorgram increase from 5 to 50 millidegree with DA concentration from 1 to 10 nM; B: from 1 to 10 nM, the sensorgram-concentration presented a linear relationship; C: the DA adsorption rate increase from 1 to 10 nM due to the reaction kinetics; D: SPR sensorgram increase from 0.005° to ~1.4° over 5 folds of DA concentration with the conjugated polymer functionalized sensor(red) while the sensorgram remained identical with PEG functionalized sensor(green); and resolution of the functionalized SPR sensor decrease with the DA concentration.

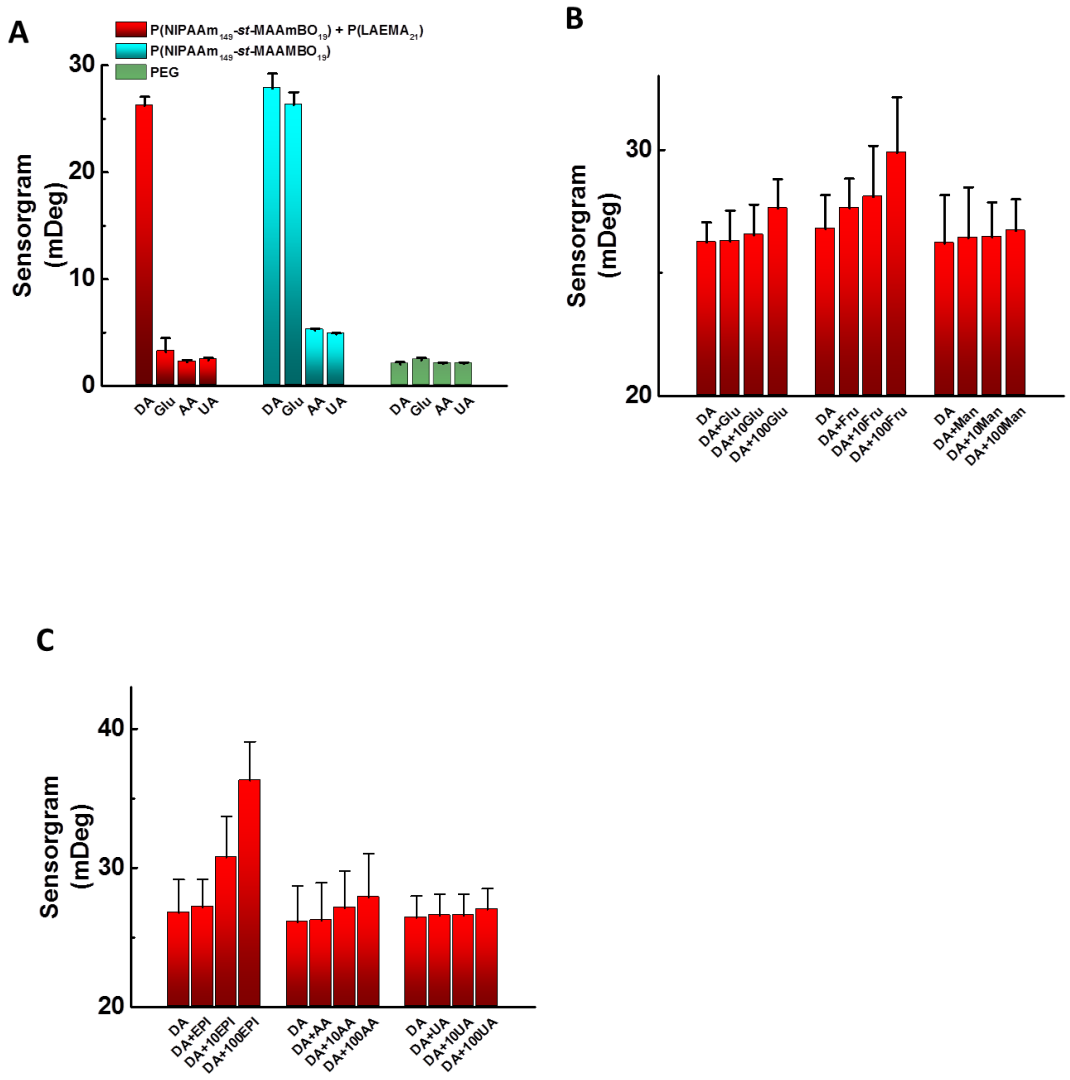

Figure 4. Selectivity and recognition test for the polymer assisted SPR sensor. A: selectivity of polymer sensing layer: with P(NIPAAm$_{149}$-*st*-MAAmBO$_{19}$) and P(LAEMA$_{21}$) functionalization, the sensor is selective to DA only; with only P(NIPAAm$_{149}$-*st*-MAAmBO$_{19}$), the sensing layer does not show any selectivity to DA; B: DA with monosaccharides; C: DA with other potential co-existed molecules and structural analogs. The functionalized polymer assay showed higher affinity toward DA than the saccharides, AA and UA, however, EPI interfered the sensorgram due to the structural similarity. All the tests are based on DA concentration of 5 nM.

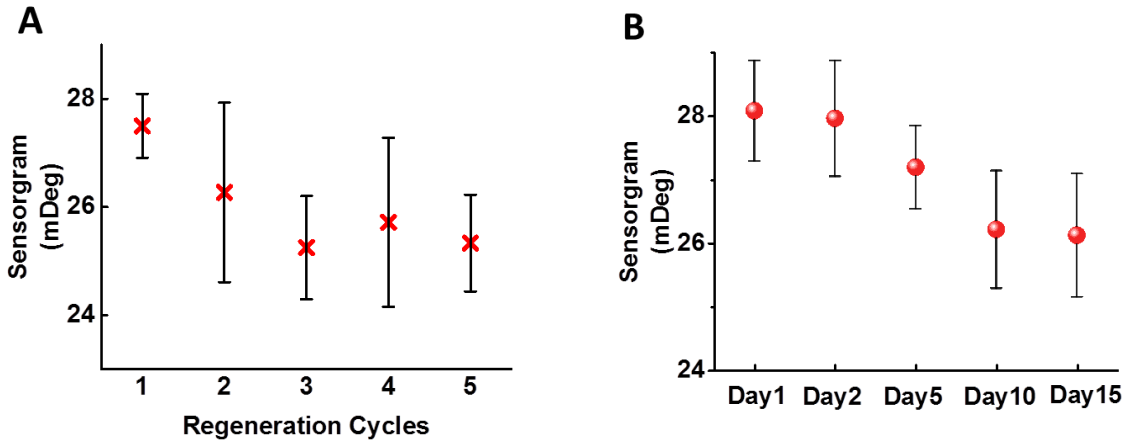

Figure 5. Sensor regeneration and stability test with 5 nM DA injections. A: SPR sensorgram signal reduced less than 10% after 5 times regeneration; B: the functionalized sensor remained 95% sensorgram signal within 5 days after surface functionalization and 90% after 15 days.

TOC